DALTON
FULL PAPER

Conformational and coordination plasticity in silver(I) cryptates

Vickie McKee,[a] Jane Nelson,[b,c] David J. Speed[b,c] and Raewyn M. Town[b]

[a] *Chemistry Dept., Loughborough University, UK, LE11 3TU*
[b] *School of Chemistry, Queens University, Belfast, UK BT9 5AG*
[c] *Open University, Milton Keynes, UK, MK7 6AA*

Received 21st May 2001, Accepted 5th October 2001
First published as an Advance Article on the web 23rd November 2001

The structure of a disilver aminocryptate with silver accommodated in the faces rather than within the tetramine-derived caps of the crypt shows close contact between Ag^+ cations indicative of interaction between the d^{10} cations. On standing in solution, a second, trisilver, cryptate is isolated, where close contact between the silver cations, now triangularly disposed, is still present. A pseudoreversible wave close to 0 V *vs.* Ag/AgCl is tentatively assigned to the one-electron I,I ↔ I,O redox process in the disilver cryptate.

The interplay of coordination preference and conformational restraint has generated not a few surprises in X-ray crystallography of copper(I) and silver(I) azacryptates.[1,2] Within iminocryptand hosts, copper(I) ions are in general restricted to coordination by the tetramine-derived N_4 caps, and while many disilver(I) complexes are isostructural with their dicopper(I) analogues, silver(I) appears ready, where necessary, to accept sites of lower donicity.[3–5] One striking example of the different strategies adopted by these d^{10} cations is illustrated by the comparison (Fig. 1) between the structures[2,4] of $[Cu_2(L^1)]^{2+}$ **1** and

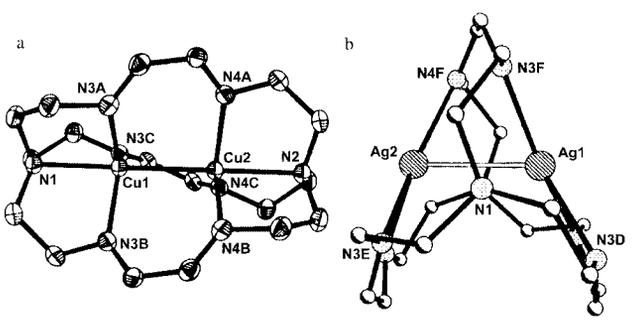

Fig. 1 Comparison of the coordination geometry for (a) $[Cu_2(L^1)]^{2+}$ **1** and (b) $[Ag_2(L^1)]^{2+}$ **2**.

$[Ag_2(L^1)]^{2+}$ **2**. Here steric constraints force the Ag(I) cations to be located in the faces rather than within the caps of the cryptand host. This facial coordination mode appears inefficient in comparison with the N_4 cap-derived site, as in contrast both to the dicopper(I) analogue and any silver(I) cryptates which utilise N_4-cap coordination sites,[1] NMR spectroscopy of **2** gives evidence[6] for decomplexation in solution.

While iminocryptands are known[1] as good ligands for M(I) cations, few complexation studies of heavy metal cations with the more basic aminocryptands have been reported, presumably because of troublesome competition with protonation equilibria. However, L^2, the aminocryptand derivative of L^1, has been shown[7,8] to act as an efficient ligand for such cations as

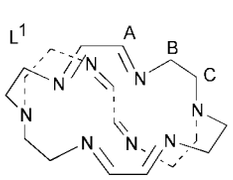

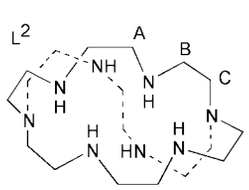

Pb(II) and Cd(II). This encouraged us to examine the complexation of silver(I) with this ligand.

Results and discussion

The initial product of reaction of Ag(I) salts with L^2 takes the form of a disilver cryptate the structure of which, shown in Fig. 2 for the fluoroborate salt $[Ag_2(L^2)](BF_4)_2$ **3**, is not radically

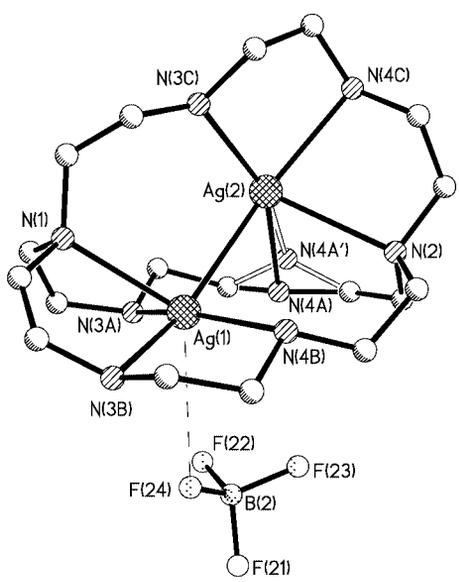

Fig. 2 $[Ag_2(L^2)]^{2+}$ cation and the weakly coordinated BF_4^- anion.

different from that found in the imino-analogue.[4] The asymmetric unit contains the $[Ag_2(L^2)]^{2+}$ cation and two BF_4^- anions, one of which interacts weakly with one of the silver ions [Ag(1)–F(24), 3.19(1) Å], as shown in Fig. 2. Selected distances and angles are given in Table 1. There is some disorder in one strand of the cage, modelled as 50% occupancy of two related sites N(4A) and N(4A′). Each silver(I) ion is coordinated to one bridgehead nitrogen, as well as to three NH donors, a pair from one strand of the cryptand as well as one each from the third strand. The Ag–N(H) distances are of the same order as Ag–N_{im} distances in iminocryptand disilver complexes[1,3–5] *i.e.* in the range 2.29–2.43 Å. AgN_{br} contacts [at 2.490(8) and 2.606(7) Å for N(1) and N(2), respectively] are longer than Ag–N(H) presumably a result of steric constraint. The main difference

DOI: 10.1039/b104434f

Table 1 Selected bond distances (Å) and angles (°) for **3** and **4**

$[Ag_2(L^2)](BF_4)_2$ **3**

Ag(1)–N(1)	2.490(8)	Ag(2)–N(2)	2.606(7)
Ag(1)–N(3A)	2.333(8)	Ag(2)–N(3C)	2.289(8)
Ag(1)–N(4B)	2.361(7)	Ag(2)–N(4C)	2.426(7)
Ag(1)–N(3B)	2.399(8)	Ag(2)–N(4A)	2.312(18)
Ag(1)–Ag(2)	2.8140(10)	Ag(2)–N(4A′)	2.239(18)
N(3A)–Ag(1)–N(4B)	156.1(3)	N(4A′)–Ag(2)–N(3C)	154.9(6)
N(3A)–Ag(1)–N(3B)	118.1(3)	N(3C)–Ag(2)–N(4A)	154.8(5)
N(4B)–Ag(1)–N(3B)	78.2(3)	N(4A′)–Ag(2)–N(4C)	112.1(6)
N(3A)–Ag(1)–N(1)	77.1(3)	N(3C)–Ag(2)–N(4C)	77.7(3)
N(4B)–Ag(1)–N(1)	126.1(3)	N(4A)–Ag(2)–N(4C)	126.4(4)
N(3B)–Ag(1)–N(1)	73.5(3)	N(4A′)–Ag(2)–N(2)	76.0(6)
		N(3C)–Ag(2)–N(2)	129.0(3)
		N(4A)–Ag(2)–N(2)	71.1(5)
		N(4C)–Ag(2)–N(2)	74.6(3)

$[Ag_3(L^2)](CF_3SO_3)_3{\cdot}H_2O{\cdot}EtOH{\cdot}0.5Et_2O$ **4**[a]

Ag(1)–N(4B)	2.164(8)	Ag(2)–Ag(3)	2.8487(11)
Ag(1)–N(3A)	2.181(7)	Ag(2)–O(31)#2	2.857(7)
Ag(1)–Ag(3)	2.8536(11)	Ag(2)–O(42)	2.931(8)
Ag(1)–O(32)	2.995(7)	Ag(3)–N(3C)	2.171(8)
Ag(1)–O(43)#1	3.167(8)	Ag(3)–N(4A)	2.178(9)
Ag(2)–N(3B)	2.168(7)	Ag(1)–Ag(2)	3.0896(11)
Ag(2)–N(4C)	2.187(7)		
N(4B)–Ag(1)–N(3A)	158.5(3)	N(4C)–Ag(2)–O(42)	71.7(2)
N(4B)–Ag(1)–O(32)	91.2(3)	N(3C)–Ag(3)–N(4A)	144.2(3)
N(3A)–Ag(1)–O(32)	71.6(2)	Ag(3)–Ag(1)–Ag(2)	57.12(2)
N(3B)–Ag(2)–N(4C)	159.3(3)	Ag(3)–Ag(2)–Ag(1)	57.27(3)
N(3B)–Ag(2)–O(42)	93.5(3)	Ag(2)–Ag(3)–Ag(1)	65.62(3)

[a] Symmetry transformations used to generate equivalent atoms: #1 $x - 1/4, -y + 1/4, z - 1/4$; #2 $x + 1/4, -y + 1/4, z + 1/4$.

between the iminocryptand analogue $[Ag_2(L^1)]^{2+}$ **2**, and this $[Ag_2(L^2)]^{2+}$ structure is that the Ag–N_{br} contact in the more flexible L^2 host can be considered as falling within bonding distance, generating a coordination number of four, if the close contact to the second silver ion is ignored, or five if it is included. Partly in consequence of hemi-coordination of counter ion by one of the Ag^+ cations, as found in the iminocryptate structure,[4] significant differences exist between the coordination geometry of the two encapsulated silver cations. The Ag–Ag distance, at 2.814(1) Å, is slightly (>0.02 Å) shorter than that seen in the L^1 analogue or in elemental silver, and is on the lower limit of such distances in disilver(I) complexes.[9]

However, despite the apparently good coordination stabilisation of this four-coordinate, interacting, silver dimer, it is not stable long-term in solution. When the L^2/Ag^+ system is allowed to stand for several days in solution, crystals of a trinuclear silver(I) cryptate can be isolated, the structure of which, as a triflate salt $[Ag_3(L^2)](CF_3SO_3)_3{\cdot}H_2O{\cdot}EtOH{\cdot}0.5Et_2O$ **4**, is shown in Fig. 3. The nuclearity of the product depends on the time allowed for rearrangement as well as, to some extent, on the ligand to silver ratio. Below an Ag : L stoichiometric ratio of 5 : 1, clean disilver cryptates were obtained as the initial product with no evidence for the presence of the trisilver cryptate.

The asymmetric unit contains a trinuclear $[Ag_3(L^2)]^{3+}$ cation, three triflate anions, one molecule each of water and ethanol and half a molecule of Et_2O (the oxygen atom of which lies on a two-fold axis). In this structure each Ag(I) is near-linear two-coordinate, when close contacts to other silver cations are ignored [Fig. 3(a)]. The Ag(I) ions each link together a pair of *sec*-amino donors from two different strands of the cryptand host; the N_{br} donors are not involved in coordination. Ag–N contacts are relatively short, and closely similar, in the range 2.164(8)–2.187(7) Å, average 2.175; there is noticeably less asymmetry in the coordinate bond distances here than in the dinuclear L^2 cryptate, **3**. Close contacts to other Ag^+ cations at 3.089, 2.849 and 2.854 Å presumably contribute to the stabilisation of the trinuclear coordination mode. These three Ag–Ag

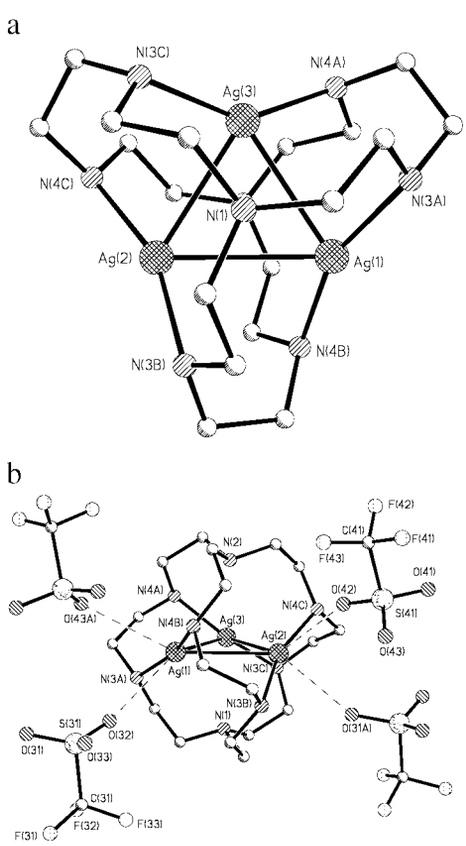

Fig. 3 (a) View down the pseudo three-fold axis of the $[Ag_3(L^2)]^{3+}$ cation. (b) Weak interactions between Ag(1) ions and triflate anions. O(31A) and O(43A) are symmetry equivalents of O(31) and O(43).

contacts suggest appreciable d^{10}–d^{10} interaction.[5] Given that the trinuclear form of this cryptate appears to be the thermodynamically stable form, the inference is that the bond energy

Table 2 MAS NMR spectra of silver and cadmium cryptates

Compound	Spectrum	ν/MHz	Reference	δ/ppm	Comment
L^2	^{13}C	75.4	TMS	56.4, 52.1, 49.0	Sharp spectrum
	^{15}N	30.4	NH_4NO_3	−339, −344, −346	Very poor noisy weak spectrum
$[CdL^2](BF_4)_2$ **5**	^{13}C	75.4	TMS	49.6, 47.5, 44.6	
	^{15}N	30.4	NH_4NO_3	−345.3(N(H)), −358.9(N_{br})	Dipolar dephasing experiment identifies N_{br}
	^{113}Cd	66.5	$CdMe_3$	65.3	No resolved ^{14}N coupling
	^{19}F	282.2	$CFCl_3$	−147.1, −153.6	
$[Ag_2(L^2)](CF_3SO_3)_2$ **3′**	^{13}C	75.4	TMS	55.1, 53.6, 49.7, 47.3	Additional poorly defined high δ shoulders
	^{15}N	30.4	NH_4NO_3	≈−350	Very weak noisy spectrum
	^{19}F	282.2	$CFCl_3$	−76.1, −77.1	Additional high δ shoulders
$[Ag_3(L^2)](CF_3SO_3)_3$ **4**	^{13}C	75.4	TMS	55.0, 53.6, 49.8, 47.4	
	^{15}N	30.4	NH_4NO_3	−346, −353	Weak noisy spectrum
	^{19}F	282.2		−76.1, −77.1	Lower δ signal more intense
	^{109}Ag	13.9	$AgNO_3$	532, 460.5	

of these Ag–Ag interactions is comparable with any Ag–N coordinate bond energy lost on formation of **4** from the dinuclear triflate, $[Ag_2(L^2)](CF_3SO_3)_2$ **3′**. Ag(1) and Ag(2) each show two weak additional interactions with oxygen atoms of two triflate ions as shown in Fig. 3(b). There are long Ag–O contacts in the range 2.857(7)–3.167(7), comparable to the Ag–F distance noted in complex **3**. These weak interactions do not involve Ag(3) or the third triflate ion which may explain the splitting of the ^{19}F resonance observed in the MAS spectrum, the difference in N–Ag–N angle at Ag(3) compared to the other two silver ions [158.5(3), 159.3(3) and 144.2(3)° for Ag(1), Ag(2) and Ag(3), respectively] and the splitting (*qv.* Table 2 and discussion below) in the ^{109}Ag resonance of **4**.

Although crystals of the trinuclear cryptate can be obtained starting with the disilver analogue, it is difficult to obtain a bulk sample of **4** uncontaminated with **3′**, so solution measurements have in general been restricted to fresh solutions of **3′**. However, in the case of solid state NMR studies where spectra of **3′** were hard to observe, being broad, weak and noisy, we have used a crude sample of **4** which C, H, N analysis and FAB MS shows to be mainly in the trinuclear form; although both tri- and di-nuclear forms will be present here, features due to the trinuclear form will dominate because they are more readily observed in this spectroscopy.

Solution ^1H NMR studies of **3′** suggest that at temperatures above ambient the cations are exchanging between cryptated and solvated environment in D_2O and CD_3CN solvents, as was observed for the L^1 analogue,[6] leaving the spectrum in the form of three broad singlets at similar, but non-identical, chemical shift to those seen in the free ligand. At temperatures close to ambient the spectrum takes the form of a broad coalesced feature with remnants of individual resonances in the 2–3.5 ppm region. However, below ≈270 K, the ^1H NMR spectrum starts to become much more complex showing that the exchange rate is now on the same order as the NMR timescale. The conformational "freezing out" of the cryptate takes place at higher temperature than in the free ligand in the same solvent system (in CD_3OD, $T_C \approx 280$ *vs.* 230 K), respectively. At 233 K, the limiting fluid temperature of CD_3CN, there are indications of partly resolved coupling in the complex spectral pattern where individual resonances, for the low symmetry environment expected on the basis of the X-ray structure, are now becoming observable. From the X-ray structure of the disilver cation $[Ag_2L^2]^{2+}$ it is clear that in the solid state one strand of the cryptand is different from the other two, doubling the possible number of resonances with respect to the symmetric host conformation, so by analogy with the conformationally frozen spectrum[7,8] of the symmetric cadmium cryptate, $[CdL^1](BF_4)_2$ **5**, at least eight methylene cap resonances and four linking ethylene resonances are possible, if the two ends of the cryptate are magnetically equivalent and if the signals can be separately resolved. In d^4-MeOD below 228 K a complex and overlapped, though individually well-resolved, set of triplet, doublet and multiplet resonances between 1.8 and 3.6 ppm (Fig. 4) represents the frozen-out cryptate spectrum. A pattern of relative intensity 1, presumably representing the single cryptand strand, is discerned in the wings of the spectrum, together with indications of appearance of an analogous pattern of relative intensity 2, before overlapping makes intensity arguments untenable. Some tentative assignments (see Table 3, Experimental section) may be made on the basis of decoupling and COSY experiments, but these can be no more than tentative given the uncertainty about the effects of slight asymmetry in the dinuclear cryptate, and also about the possibility of the existence of more than one conformation in solution, as noted in other disilver cryptates we have studied.[3,5] Given the complexity of the frozen-out dinuclear spectra, solution NMR studies were restricted to **3′**.

MAS-CP NMR spectra (Table 2) were obtained for both the pure di- and the crude tri-silver cryptates in the solid state. The ^{13}C spectra are broad but complex; contributions from at least six/seven separate resonances in the spectral range 40–60 ppm are evident, although the breadth of the signals and the degree of overlapping precludes their analysis into individual components. The more symmetric trinuclear cryptate does appear to present the sharper and simpler spectrum but both dinuclear and trinuclear cryptates show four clear maxima close to 47, 50, 54 and 55 ppm. This compares with three lines, 49.0, 52.1 and 56.4 ppm for the free cryptand and, at 5–6 ppm lower frequency (in response to coordination of the positively charged cation) for the monocadmium cryptate **5**. In both these cases only three separate resonances expected for methylene carbons A, B and C in the symmetric conformation known to exist in the solid state[7,10] can be seen.

The ^{15}N spectra are more clearly defined for the trinuclear complex **4**, where peaks close to −346 and −353 ppm can be seen. In the disilver cryptate, **3′**, there are indications of two pairs of lines centred around −343 and −350 ppm, but the assignment is tentative only, because of poor signal to noise ratio. The free cryptand L^2 also presents a very poor ^{15}N spectrum, with indications of four components in two pairs of resonances centred at ≈−339 and ≈−346 ppm.

In comparison the MAS-CP ^{15}N spectrum of **5** is strong and simple with components at around −345 ppm for the secondary amino N and −359 ppm for the non-protonated bridgehead N, as shown by a dipolar decoupling experiment. While the poor quality of free ligand spectrum hinders evaluation of coordination shifts, it is at least clear that no large coordination shifts in the ^{15}N resonance are apparent. In the iminocryptand analogue L^1, sizeable ^{15}N coordination shifts[6] are noted for both the silver cryptate (at ≈30–55 ppm) and cadmium cryptate (at ≈57–54 ppm) resonances. The ^{113}Cd signal appears as a strong unsplit 65.3 ppm singlet in **5**, compared to 93.7 ppm in the L^1 analogue,[6] with no indication of the coupling to N-donors which was so evident in the latter case.

Table 3 ^{1}H NMR: partial and tentative assignment of 228 K spectrum of **3′**

δ/ppm (J/Hz)	Integral	Coupling *via* COSY	Decoupling[a]	Tentative assignment
3.53, tr (13.2)	1	≈3.15 and ≈2.55	(2.4–2.6) and (3.0–3.2) resonances simplified	HB_{ax}
3.35, dd (≈14, ≈6)	1	≈2.2	[b]	HA′[c]
2.23, dd (14.2, 5.8)	1	≈3.3	3.35 d (collapses to a singlet)	HA″[c]
1.81 d (12.6)	1	(3.0–3.2)	(3.0–3.2) simplified	HC_{eq}
3.0–3.2, m[d]	[e]	≈1.8, ≈3.5 *inter alia*	1.81 d collapsed to singlet on 3.13 irradn.	Contains HC_{ax}
2.4–2.6, m[d]	[e]	≈3.5, *inter alia*	3.53 tr collapsed to doublet on 2.65 irradn.	Contains HB_{eq}

[a] Effect of irradiation at the chemical shift specified in column 1. [b] Not attempted (too close to solvent resonance). [c] A′, A″ cannot be differentiated as axial or equatorial signals. [d] Overlapping prevents integration. [e] Complexity prevents estimation of J.

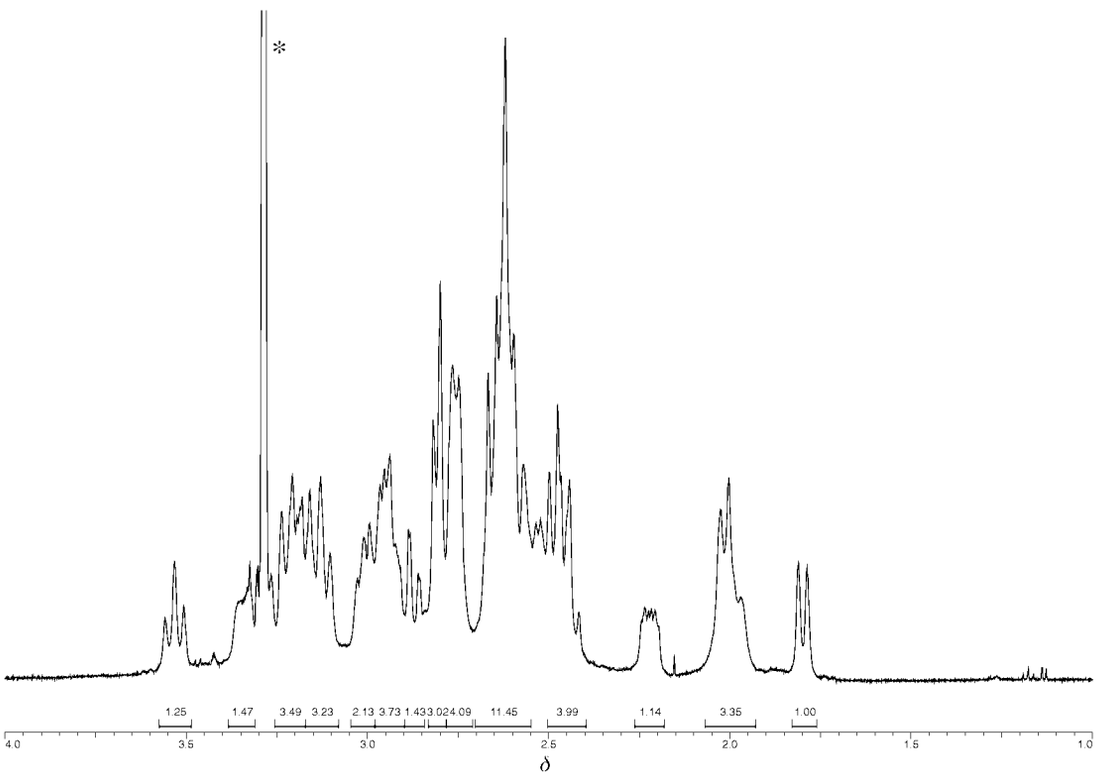

Fig. 4 ^{1}H NMR spectrum of $[Ag_2(L^2)](CF_3SO_3)_2$ **3′** in CD_3OD at 228 K with integral values indicated below each feature.

^{19}F MAS-CP resonances are split by over 6 ppm in the cadmium fluoroborate salt, **5**, indicating inequivalent siting of anions in the lattice of the cadmium salt, where the crystallographic independence of the two BF_4^- anions has been demonstrated.[7] The ^{19}F spectra of **3** and **4** also show small (≈1 ppm) splitting of the ^{19}F resonance arising presumably from the coordination inequivalence of the triflate anions mentioned above.

Despite the insensitivity of the nucleus, we did succeed in obtaining a ^{109}Ag MAS spectrum for the trimeric cryptate **4**. This consisted of a pair of resonances of similar intensity, at 460 and 532 ppm from the $AgNO_3$ standard. It is known[11] that ^{109}Ag MAS NMR is very sensitive to small changes in coordination geometry, and the asymmetry in the Ag_3 triangle, where the Ag(1)–Ag(2) distance is ≈0.2 Å longer than the other [Ag(2)–Ag(3) and Ag(1)–Ag(3)] distances, demonstrates a different geometric environment for the Ag(3) cation, which together with the differential triflate coordination presumably explains this splitting.

Electrochemistry

The lability of the complexes illustrated by their NMR spectra presents difficulty for interpretation of solution properties. However, given the possibility of observation of unusual redox states, we thought it worthwhile to examine their electrochemistry. For comparison we initially examined $[Ag_2L^1]^{2+}$ as well as $[Ag_2L^2]^{2+}$ in acetonitrile solution. At 295 K, the voltammograms examined over the range −1.6 to +2.0 V were broad, irreversible and prone to stripping phenomena. In addition to the stripping peak close to 0.5 V, irreversible oxidation waves were seen on a Pt electrode around +1.4 and near +2 V (this as a broad shoulder on solvent wave) for $[Ag_2L^1]^{2+}$ and +1.1 to 1.4 V (with reference to Ag/AgCl) for $[Ag_2L^2]^{2+}$. In reduction, a pair of broad ill-defined irreversible waves were seen close to −0.3, −0.8 V for $[Ag_2L^1]^{2+}$ and around −0.4 to −1.3 V for $[Ag_2L^2]^{2+}$. The potential differences between observed features (which are admittedly broad and ill-defined) suggest that the ligand has some control over the redox processes.

In an attempt to reduce the problem with silver deposition and stripping by slowing down the exchange process the voltammograms were run at low temperature in butyronitrile using a CO_2-snow cooling bath. Under these circumstances, the stripping problem was less marked, but quality of the voltammograms deteriorated as the faradaic current diminished in response to slower diffusion rates, and they were in general unusable by temperatures where the ^{1}H NMR spectra showed conformational freezing.

Better voltammograms were obtained in propylene carbonate, although the same diminution of faradaic current resulted from running below 273 K, so scans run between 290 and 280 K provided the most useful information. Once more these showed considerable similarity to the behaviour of simple silver salts in

this medium, indicating that dissociation may be contributing to the complexity of the voltammograms. In addition to the stripping peak centred about +0.5 V, which was characterised, in rotating disc electrode scans, by strong features typical of an accumulation process, there are, for $[Ag_2L^2]^{2+}$, three main regions of electroactivity: (i) +1.1 to +1.6 V: irreversible oxidations observed as strong and broadly structured features. (ii) −0.4 to −1.5 V irreversible reductions linked to a scan-rate dependent irreversible oxidation component centred around −0.2 V. (iii) Where stripping problems are avoided by restricting the potential to below +0.5 V, a pseudo-reversible wave was centred just negative (−0.03 V) of 0 V.

The features (i) are more intense and more richly structured than in solvated Ag^+ and are not associated with adsorption phenomena. Compared with solvated Ag^+ systems, they lie to less positive potential by around 0.2–0.3 V.

The ill-defined irreversible reduction wave at potential more negative than −1 V appears similar to that seen in solvated Ag^+ and in $[AgL^1]$; however as the −0.8 V reduction feature is absent from the solvated Ag^+ system, it presumably originates in redox of cryptated disilver.

Solvated Ag^+ shows no electroactivity when scanned over the region −0.4 to +0.4 V (Fig. 5). This confirms that the pseudo-

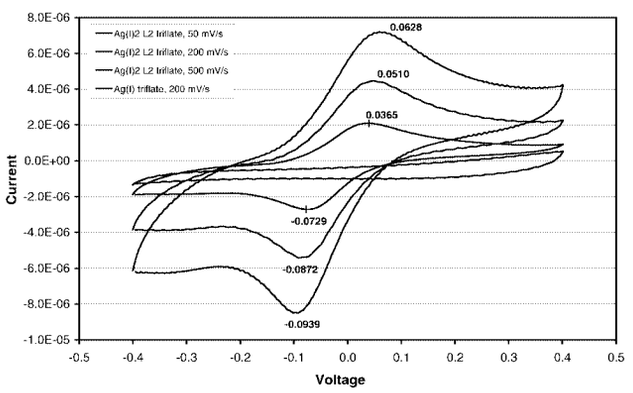

Fig. 5 Cyclic voltammograms for 1.05 mM $[Ag_2(L^2)](CF_3SO_3)_2$ **3′** in propylene carbonate; comparison of scan rates: 50, 200 and 500 mV s^{-1}, Pt electrode, 0.1 M tetrabutylammonium perchlorate supporting electrolyte.

reversible wave centred around −0.03 V derives from redox of the disilver cryptate. The most likely candidate for a redox process close to 0 V is a one-electron reduction of the disilver Ag(I)Ag(I) assembly to Ag(I)Ag(0). Attempts at further reduction to *e.g.* Ag(0)Ag(0) resulted only in the appearance of the familiar deposition/stripping features, which, lying so close in potential to the −0.03 V reduction, are likely to present difficulty in any attempt at bulk isolation of the Ag(I)Ag(0) product.

Experimental

The free cryptands were made as described in earlier papers,[3,4] while **2** was made as described earlier.[4]

$[Ag_2(L^2)](BF_4)_2$, 3

This was made by treating L^2 (37 mg, 0.1 mmol) dissolved in 3 cm^3 MeOH with 55 mg (0.28 mmol) $AgBF_4$ and filtering off the precipitated black silver oxide. On standing overnight in an ether bottle, X-ray quality crystals of **3** were obtained. The composition of these crystals was unaffected by stoichiometry up to Ag : L ratios of 5 : 1 [Found (calc.): C, 28.5 (28.5); H, 5.6 (5.6); N, 14.4 (14.8)%]. FAB-MS: *m*/*z* AgL 477 (100); $Ag(L)BF_4$ 565 (12); Ag_2L 585 (10); $Ag_2(L)BF_4$ 673(5) (relative intensities in parentheses).

$[Ag_2(L^2)](CF_3SO_3)_2$, 3′

This was made using $AgCF_3SO_3$ in place of $AgBF_4$: 140 mg (0.38 mmol) of L^2 was dissolved in 5 mL of isopropyl alcohol, and the solution placed in a foil covered vessel. Nitrogen was bubbled through the solution for 10 min, and then 400 mg (1.56 mmol) of solid silver trifluoromethanesulfonate was added, and a foil cover placed over the top of the vessel. The gas flow was continued for another 30 min, and the vessel was then left sealed overnight. The pale yellow supernatant was transferred to a clean vial, and crystals were obtained by the slow diffusion of diethyl ether into the solution. Yield 182 mg (0.21 mmol, 54%). FAB-MS: *m*/*z* AgL 477 (100); $AgL(CF_3SO_3)$ 627 (19); Ag_2L (CF_3SO_3) 735 (10) (relative intensities in parentheses) [Found (calc.): C, 27.3 (27.2); H, 5.0 (4.8); N, 12.6 (12.7)%].

$[CdL^2](BF_4)_2$ 5

This was made[7,8] as previously described. FAB-MS: *m*/*z* CdL 483 (100) $Cd(L)BF_4$ 569 (50); $Cd(L)BF_4(BF_3)$ 635 (20) (relative intensities in parentheses).

$[Ag_3(L^2)](CF_3SO_3)_3$, 4

$[Ag_3(L^2)](CF_3SO_3)_3$, was prepared using the following procedure: 70 mg (0.19 mmol) of L^2 was dissolved in 5 cm^3 isopropyl alcohol, and the solution placed in a foil covered vessel. Nitrogen was bubbled through the solution for 10 min, and then 194 mg (0.76 mmol) of solid silver trifluoromethanesulfonate was added, and a foil cover placed over the top of the vessel. The gas flow was continued for another 30 min, and the vessel was then left sealed in the dark for 9 days. A colourless solution with an insoluble black solid was obtained after this time, the supernatant solution was transferred to a clean vial, and crystals were obtained by the slow diffusion of diethyl ether into the solution. Yield 56 mg (0.05 mmol, 26%). FAB-MS: *m*/*z* AgL 477 (100); $AgL(CF_3SO_3)$ 627 (1); $Ag_2L(CF_3SO_3)$ 735 (37); $AgL(CF_3SO_3)_2$ 779 (1); $Ag_2L(CF_3SO_3)_2$ 884 (1.5); $Ag_3L(CF_3SO_3)_2$ 990 (2) (relative intensities in parentheses) [Found (calc.): C, 21.97 (22.10); H, 3.76 (3.71); N, 9.69 (9.82)%]. The bulk sample used for MAS NMR had the following percentage C, H, N composition 21.65; 3.66; 9.12.

NMR spectroscopy

Solution NMR spectra were recorded on a Bruker 500 MHz instrument at QUB in d_4-methanol (Apollo Scientific Ltd). A summary of results, and the frequencies used for decoupling experiments is given in Table 3. Chemical shifts are given in parts per million (ppm, δ) with tetramethylsilane (TMS) as an internal standard. MAS conditions are listed in Table 2.

Electrochemistry

Cyclic voltammetry was performed with an AUTOLAB PGSTAT10 potentiostat, using a stationary or rotating Pt disk working electrode (diameter 2.5 mm), Ag/AgCl reference, and Pt counter electrodes. Solutions of AgL (*ca.* 10^{-3} mol dm^{-3}) were prepared in propylene carbonate or acetonitrile containing 0.1 mol dm^{-3} $(C_4H_9)_4NClO_4$ (Fluka, purum) as supporting electrolyte. Oxygen-free nitrogen was bubbled through solutions before analysis, and a positive nitrogen pressure was maintained over the solution during all measurements. The working electrode was periodically cleaned by dipping in conc. HNO_3. All solvents were spectroscopic grade.

X-Ray experimental

Both data sets were collected on a Siemens P4 diffractometer using Mo-Kα radiation, complex **3** at room temperature and complex **4** at 153(2) K. Both were solved by Patterson methods and refined by full-matrix least-squares on F^2 using SHELXTL.[12] Details of the data collections and structure

Table 4 X-Ray data collection and structure refinements

	$[Ag_2(L^2)](BF_4)_2$	$[Ag_3(L^2)](CF_3SO_3)_3 \cdot H_2O \cdot EtOH \cdot 0.5Et_2O$
Formula	$C_{18}H_{42}Ag_2B_2F_8N_8$	$C_{24}H_{53}Ag_3F_9N_8O_{11.50}S_3$
M	759.96	1228.53
Crystal system	Monoclinic	Orthorhombic
Space group	$P2_1/n$	$Fdd2$
a/Å	16.4970(10)	33.920(6)
b/Å	9.517(2)	43.787(3)
c/Å	17.971(2)	11.445(2)
β/°	94.13	90
U/Å^3	2814.2(7)	16999(4)
Z	4	16
μ(Mo-Kα)/mm^{-1}	1.469	1.617
Reflections collected	5781	4206
Independent refl. (R_{int})	4943 (0.0378)	3955 (0.0271)
$R1$, $wR2$ indices [$I > 2\sigma(I)$]	0.0628, 0.1636	0.0413, 0.0660
$R1$, $wR2$ indices (all data)	0.0884, 0.1842	0.0615, 0.0717
Abs. structure parameter	—	0.02(4)

refinements are given in Table 4 and selected bond lengths and angles are listed in Table 1.

CCDC reference numbers 167460 and 167461.

See http://www.rsc.org/suppdata/dt/b1/b104434f/ for crystallographic data in CIF or other electronic format.

Acknowledgements

We wish to thank EPSRC for access to the FAB-MS service at Swansea and the Solid State NMR service at Durham. We are grateful to the Open University Research Committee for funding for a Postgraduate Studentship (to D. S.).

References

1 J. Nelson, V. McKee and G. G. Morgan, *Prog. Inorg. Chem.*, 1998, **47**, 167.
2 C. J. Harding, V. McKee and J. Nelson, *J. Am. Chem. Soc.*, 1991, **113**, 9684.
3 O. W. Howarth, V. McKee, G. G. Morgan and J. Nelson, *J. Chem. Soc., Dalton Trans.*, 1999, 2097.
4 J. L. Coyle, V. McKee and J. Nelson, *Chem. Commun.*, 1998, 709.
5 D. Farrell, M. G. B. Drew, V. McKee, G. Morgan and J. Nelson, *J. Chem. Soc., Dalton Trans.*, 2000, 1513.
6 D. C. Apperley, W. Clegg, S. Coles, J. L. Coyle, N. Martin, B. Maubert, V. McKee and J. Nelson, *J. Chem. Soc., Dalton Trans.*, 1999, 229.
7 J. A. Thompson, M. E. Barr, D. K. Ford, L. A. Silks, B. J. McCormick and P. H. Smith, *Inorg. Chem.*, 1996, **35**, 2025.
8 N. Martin, V. McKee and J. Nelson, *Inorg. Chim. Acta*, 1994, **218**, 5.
9 P. Pyykko, *Chem Rev.*, 1997, **97**, 597.
10 P. H. Smith, M. E. Barr, J. R. Brainard, D. K. Ford, H. Frieser, S. Muraldiharar, S. D. Reilly, R. R. Ryan, L. A. Selles and W. H. Yu, *J. Org. Chem.*, 1993, **58**, 7939.
11 H. G. Fijolek, T. A. Oriskovich, A. J. Benest, P. Gonzalez-Duarte and M. J. Natan, *Inorg. Chem.*, 1996, **35**, 797.
12 G. M. Sheldrick, SHELXTL Version 5.1, Bruker AXS, Madison, WI, 1998.